3.01 Basic Aspects of Membrane Reactors

J Caro, Leibniz Universität Hannover, Hanover, Germany

3.01.1 Introduction

The conversion and selectivity of a chemical reaction can be improved when the reaction is performed in a membrane reactor. A membrane reactor is a bifunctional apparatus combining a membrane-based separation with a (catalytic) chemical reaction in one device [1]. There are some recent reviews showing the benefits of a membrane-supported chemical reaction [2–14]. Membrane-supported operations and membrane reactors will play an important role in process intensification; for example, membrane contactors are reactor concepts with a high feasibility [15–17]. Many chemical processes of industrial importance, classically using fixed-, fluidized-, or trickle-bed reactors, involve the combination of high temperature and chemically harsh environment that favor inorganic membranes [14]. However, as yet no inorganic membranes are used in large-scale industrial gas separation and no high-temperature chemical membrane reactor is in operation. On the contrary, in biotechnology, a beginning of the exploitation of both organic and inorganic membrane reactor technology in low-temperature applications can be stated [18–19].
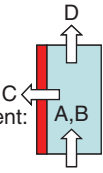
There are numerous concepts to classify membrane reactors following, for example, the reactor design such as extractors, distributors, or contactors, dividing the membrane into inorganic and organic ones or porous and dense ones, using the reaction types such as oxidations, hydrogenations, isomerizations, and esterifications, defining inert or catalytic membrane reactors, or taking as classification principle the position of a catalyst in/near/before/behind a membrane. Different to these sophisticated concepts, in this chapter, a simple classification of membrane reactors into only two groups is used (as shown in **Table 1**):

1. *Conversion enhancement in extractor-type membrane reactors operating thermodynamically near/at reaction equilibrium.* To overcome the equilibrium

Table 1 Classification of membrane reactors used in this chapter

Thermodynamically controlled reactions	*Kinetically controlled reactions*
$\Delta_R G^0$ near zero	$\Delta_R G^0$ very negative
$\Delta_R G^0 = -RT \ln K \rightarrow K \approx 1$	$\Delta_R G^0 = -RT \ln K \rightarrow K \gg 1$
$A + B \leftrightharpoons C + D$	$A + B \rightarrow C + D$
Extractor type membrane reactor Conversion enhancement: Dehydrogenation Esterification Steam reforming Knoevenagel condensation Water splitting	*Distributor/contactor type membrane reactor* Selectivity enhancement: Hydrocarbon oxidation p-Xylene oxidation Methane to synthesis gas Partial hydrogenation

restriction, the reaction must be sufficiently fast compared to the mass transport through the membrane (kinetic compatibility). A special advantage can be that the removal of one of the products provides an integrated product purification, thus decreasing the number of process units. Besides, selectivity improvements can be found by selectively removing reaction rate inhibitors [20].

2. *Selectivity enhancement in distributor/contactor-type membrane reactors operating under reaction kinetics-controlled conditions.* The desired product is usually an intermediate in a consecutive reaction, or is one of the products in a system of parallel reactions. One should note that in the case of a distributed feed along the reactor, the flow rate downstream usually increases and the residence time at the catalytic sites will be reduced.

p0015 Because of the worldwide intense research and development (R&D) on membrane reactors and the corresponding large number of publications and patents, only characteristic examples for the two principles are discussed and emphasis is given to recent literature after 2000. Further, the successful use of an extractor-type membrane reactor in the decomposition of NO_x into the elements N_2 and O_2 is described. Here, the product molecule oxygen acts as a reaction rate inhibitor, which can be *in situ* removed using an oxygen-transporting perovskite membrane.

3.01.2 Conversion Enhancement in Extractor-Type Membrane Reactors Operating Thermodynamically under Equilibrium-Controlled Reaction Conditions

s0010

3.01.2.1 Boosting of Alkane Dehydrogenation by Hydrogen Removal

s0015

There are numerous examples for the conversion p0020 enhancement of an alkane dehydrogenation using porous (zeolite and sol–gel metal oxide) or dense (metal and ceramic) hydrogen-selective membranes. The concept to increase the alkane conversion by selectively removing the hydrogen seems to be simple at first sight; however, there can be a number of implications, such as coking, hydrogenolysis, and cracking [2], in the usual tubular membrane reactors for dehydrogenation (**Figure 1**). Further, if pore membranes are used and a light sweep gas such as He is applied to reduce the hydrogen partial pressure on the permeate side, the crossover of the sweep gas by counter-diffusion from the sweep to the feed side

Conventional fixed bed

i-butane → Cr₂O₃ / Al₂O₃ → i-butene
i-butane
H₂

Fixed bed with membrane

i-butane → Cr₂O₃ / Al₂O₃ → i-butene
i-butane
↓ H₂
Sweep gas N₂
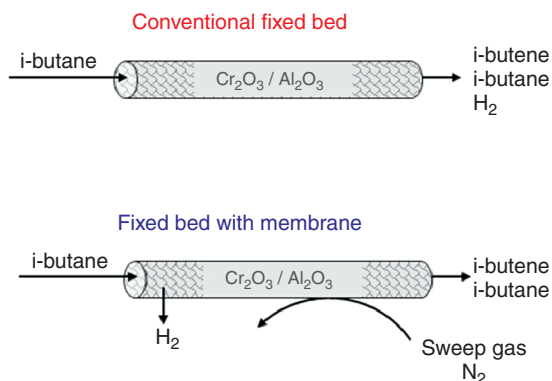
Figure 1 Typical experimental setup used for the membrane-supported dehydrogenation of alkanes using tubular hydrogen-selective membranes. Overlapping processes of dehydrogenation with cracking, coking, hydrogenolysis, and dilution of the feed by the sweep gas can falsify the results (see text).

of the membrane must be avoided since the dilution of the alkane on the feed side by the sweep gas also increases the conversion of the alkane dehydrogenation.

p0025 On the other hand, it is not compulsory to use narrow-pore membranes with pores only accessible for hydrogen. In addition, medium-pore zeolite membranes, the pore size of which allows the passage of both hydrogen and the hydrocarbons, can be used successfully in the membrane-supported dehydrogenation. As an example, a MFI zeolite membrane is used in the catalytic dehydrogenations of i-butane. Despite the fact that both H_2 and i-butane can pass the 0.55-nm pores due to their kinetic diameters (0.29 and 0.50 nm, respectively), the interplay of mixture adsorption and mixture diffusion results in a H_2 selectivity at high temperatures (H_2 flux $\approx 1 \, m^3 \, m^{-2}$ h^{-1} with a mixture separation factor α (H_2/i-butane ≈ 70 at $500 \, °C$) and in an i-butane selectivity of the silicalite-1 membrane at low temperatures (i-butane flux $\approx 0.5 \, m^3 \, m^{-2} \, h^{-1}$ with a mixture separation factor α (i-butane/$H_2 \approx 15$ at room temperature) [21].

In the conventional packed-bed experiment, the thermodynamic equilibrium conversion was obtained (**Table 2**). As hydrogen was removed selectively through the silicalite-1 membrane, the i-butane conversion increased by about 15% [21]. The removal of hydrogen leads to hydrogen-depleted conditions, which have two positive effects: (1) the conversion of i-butane is increased as expected due to a lower rate of the reverse reaction and (ii) the selectivity to i-butene is also increased because the hydrogenolysis is suppressed. Therefore, at the beginning of the reaction the i-butene yield in the membrane reactor is higher by about $1/3$ than in the conventional packed-bed (**Table 2**). However, because of the hydrogen removal, coking is promoted and after approximately 2 h time on stream the olefin yield of the membrane reactor drops below that of the classical packed bed [22]. However, after an oxidative regeneration, the activity and selectivity are restored completely. Further experimental results for the silicalite-1-assisted dehydrogenation of i-butane can be found, for example, in References 22 and 23.

p0030 Future developments of membranes for hydrogen economy could trigger new activities in the membrane-supported dehydrogenation. Most promising seems to be the development of thin (about 1 µm) supported hydrogen-selective zeolite layers on a wide variety of carriers, for example, capillaries, fibers, tubes, or monoliths, such as the synthesis of thin zeolite layers on spun hollow fibers as support [24]. Since Si-rich zeolite membranes are hydrothermally more stable, Corma's full SiO_2 with lipoteichoic acid (LTA) structure (ITQ 29) [25] AU5 would be a promising candidate for a hydrogen-selective membrane development and first attempts can be stated [26]. In addition, the synthesis of one-dimensional (1D) $AlPO_4$-5 membranes with a c-out-of-plane orientation of the parallel AFI pores by tertiary growth, is a pioneering concept for developing 1D membranes for hydrogen sieving [27].

t0010 **Table 2** Increase of the i-butane conversion X(i-butane) above the equilibrium limit if hydrogen is removed through a silicalite-1 membrane

Temperature (°C)	X(i-butane) (%)	
	Classical packed bed	Membrane supported packed bed
510	35	39
540	43	60

Conditions: WHSV = 1 h⁻¹, Cr₂O₃/Al₂O₃-catalyst (Süd-Chemie), membrane area per unit mass of catalyst = 20 cm² g⁻¹, data after 20 min time on stream. From Illgen, U., Schäfer, R., Noack, M., Kólsch, P., Kúhnle, A., Caro, J. *Catal. Commun.* **2001**, *2*, 339.

Six-ring zeolite membranes, such as SOD (0.28-nm pore size), and 8-ring zeolite membranes, such as CHA (0.34 nm) and deca-dodecasil 3R (DDR; 0.44 nm), will allow the effective separation of hydrogen.

s0020 3.01.2.2 Increasing the Esterification Yield by Water Removal

p0035 With the availability of water selective membranes, which are stable in acidic surrounding and organic solvents at elevated temperatures, membrane-supported esterification becomes possible. There are different ways to increase the yield of an esterification. Most frequently, the cheapest educt is present in a surplus concentration or the low boiling ester is removed by reactive distillation. Another concept is to keep the concentration of the product water as low as possible by the use of adsorbents such as LTA zeolites or even by chemical reactions such as the hydrolysis of Al tri-isopropylate, thus consuming water. In the case of the low-temperature esterification of methanol or ethanol with short-chain monovalent hydrocarbon acids, hydrophilic organic polymer membranes can be used for the *in situ* dewatering in a membrane reactor. However, to support esterifications at higher temperatures, hydrophilic inorganic membranes with high stability against strong acids have to be used. ZSM-5-type zeolite membranes are suitable candidates to fulfill these demands. The benefits of a membrane-supported esterification were shown for the reaction of *n*-propanol with propionic acid using a ZSM-5 membrane of the $Si/Al = 96$. The ester yield can be increased from 52% to 92% by removal of water through the membrane (**Figure 2**). This ZSM-5 membrane is acid stable up to $pH = 1$; however − due to the low Al-contents − the hydrophilicity is low and, consequently, the resulting water flux of $72 \, \text{g m}^{-2} \, \text{h}^{-1} \, \text{bar}^{-1}$ is still much too low for technical applications.

p0040 There is ongoing research on novel water selective membranes. A recently developed phillipsite (PHI) membrane with a mixture separation factor $\alpha > 3000$ for a 10 wt.% water/90 wt.% ethanol mixture with water fluxes $>0.3 \, \text{kg m}^{-2} \, \text{h}^{-1}$ looks promising [28]. In another application for the selective removal of water by pervaporation and vapor permeation during an esterification by using hydrophilic ZSM-5 and mordenite (MOR) membranes, almost complete conversion of about 100% was reached within 8 h in the esterification of lactic acid with ethanol [29]. Vapor permeation is also applicable to the *in situ* removal of water in the formation of unsaturated polyesters [29].

p0045 Conventionally, only hydrophilic membranes are used for dehydration of solvents. Despite its hydrophobic character, the all-silica DDR membrane turns out to be well suited to separate water from organic solvents by molecular sieving due to its small pore size [30]. Excellent performance in the dewatering of
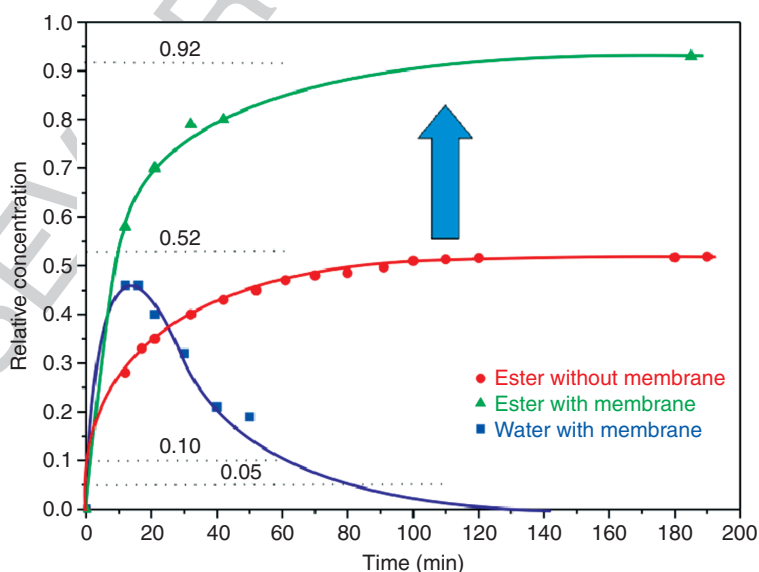
f0010 **Figure 2** Conversion enhancement by water removal via a hydrophilic ZSM-5 membrane with a $Si/Al = 96$ in a membrane reactor for the esterification reaction of propionic acid + i-propanol ⇆ ester + water at 70 °C [36].

ethanol (flux of $2 \, kg \, m^{-2} \, h^{-1}$ and $\alpha = 1500$) is observed and the membrane is also able to selectively remove water from methanol (flux of $5 \, kg \, m^{-2} \, h^{-1}$ and $\alpha = 9$). Water could also be removed from methanol/ethanol/water mixtures, even at water feed concentrations below 1.5 wt.%. This water removal by DDR membranes is attributed to molecular sieving. Water easily passes through the DDR structure, while the organic molecules experience increasing diffusion hindrance with increasing size.
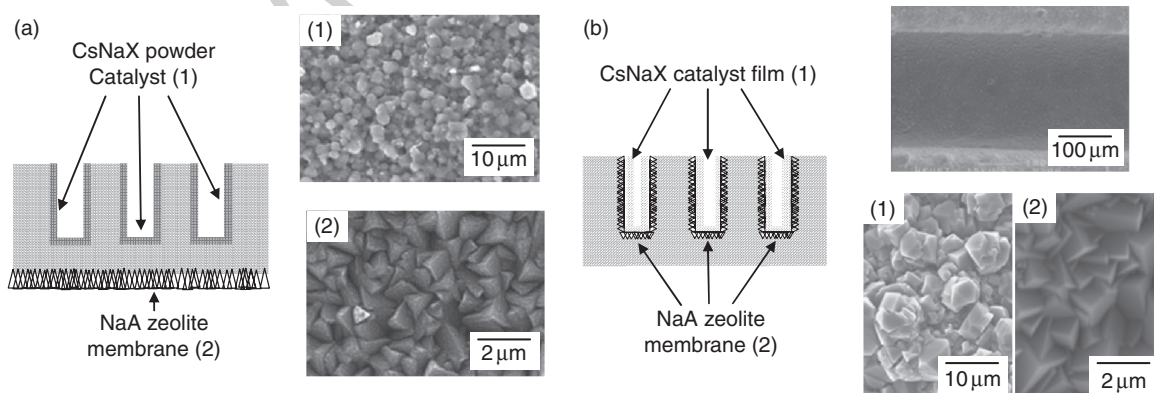
p0050   In the Fischer–Tropsch synthesis, the removal of the by-product water has several advantages on the reactor performance, such as reduced catalyst deactivation and lowered kinetic inhibition. Therefore, it was proposed to use hydrophilic membranes to increase reactor productivity [31]. The *in situ* water removal by a sol–gel silica-based membrane [32] and a ceramic-supported polymer membrane [33] in the presence of a CO/CO_2-shift active Fe-based catalyst resulted in increased total carbon conversion to hydrocarbons. The application of more hydrophilic zeolite membranes than silica or organic polymers with higher selectivity and higher water fluxes, such as LTA [34] and H-SOD [35], for the *in situ* water removal in Fischer–Tropsch synthesis looks promising.

s0025 **3.01.2.2.1 *Water removal in Knoevenagel condensations in micro reactors***

p0055 The Knoevenagel condensation is a modification of the aldol condensation named after Emil Knoevenagel. It is a nucleophilic addition of an active hydrogen compound to a carbonyl group followed by a dehydration reaction in which a molecule of water

is eliminated (hence condensation). The combination of the concepts of membrane reactor and process miniaturization provides new routes for chemical synthesis that promises to be more efficient, cleaner, and safer [37]. These smart, integrated, microchemical systems are expected to bring into realization a distributed, on-site, and on-demand production for high value-added products in the form of miniature factories and micro-pharmacies [38]. The incorporation of zeolites in microreactors as functional elements, including catalysts [39–41] and membranes, has been reported in previous works [42–44].

A recent example of fine chemical reaction carried p0060 out in a membrane microreactor is the Knoevenagel condensation reaction where the selective removal of the by-product water during the reaction led to a 25% improvement in the conversion [45]. The reaction between benzaldehyde and ethyl cyanoacetate to produce ethyl-2-cyano-3-phenylacrylate was catalyzed by a CsNaX zeolite catalyst deposited on the microchannel and the water was selectively pervaporated across an LTA membrane (**Figure 3**(**a**) [46]. All the water produced by the reaction was completely removed and the membrane was operating below its capacity [47]. This means that the performance of the membrane microreactor is limited mainly by the kinetics, that is to say that both thermodynamic and mass transfer constraints were removed. A fourfold increase in reaction conversion was obtained when the improved CsNaX–NH_2 catalyst was used instead of CsNaX [48]. Locating the separation membrane immediately next to the catalyst further improved the membrane microreactor performance (**Figure 3**(**b**)). The selective removal of the by-

f0015 **Figure 3** Membrane microreactor for Knoevenagel condensations with water removal [45, 46]: (a) The CsNaX catalyst (1) is deposited as powder on the microchannel wall and the 6-μm-thick NaA membrane (2) is grown on the back of the stainless steel plate. (b) The CsNaX catalyst film (1) is deposited directly on top of the 6.5- μm-thick NaA membrane (2) in the microchannel.

product water in the membrane microreactors also benefited other Knoevenagel condensation reactions, such as reactions between benzaldehyde and ethyl acetoacetate and diethyl malonate [49].

p0065 A multichannel membrane microreactor for the continuous selective oxidation of aniline by hydrogen peroxide on TS-1 nanoparticles was successfully AU6 demonstrated. The high surface-area-to-volume ratio that can be attained in the microreactor ($3000\,m^2\,m^{-3}$) facilitates the selective removal of the water by-product, which reduces also the catalyst deactivation during the reaction. An improvement in the product yield and selectivity toward azoxybenzene was also observed. Azobenzene was obtained as by-product and its formation was attributed to the homogeneous reaction of nitrosobenzene with aniline. Increasing temperature was beneficial for both yield and selectivity; however, beyond 67°C, microreactor operation was ineffective due to bubble formation and hydrogen peroxide decomposition [50, 51].

s0030 ### 3.01.2.3 Hydrogen Production by Water Splitting Using Oxygen-Selective Perovskite Membranes

p0070 Recently, it was shown that it is possible to produce significant amounts of hydrogen from water splitting at around 900 °C, using a novel $BaCo_xFe_yZr_zO_{3-\delta}$ (BCFZ) oxygen-permeable hollow-fiber membrane [52]. Although water dissociation into oxygen and hydrogen is conceptually simple, efficient hydrogen production from water remains difficult due to the small equilibrium constant of water dissociation $H_2O \rightleftarrows H_2 + \frac{1}{2}O_2$. Because of the low $K_p \approx 2 \times 10^{-8}$ at 900 °C only tiny equilibrium concentrations of $P_{O2} \approx$

4.6×10^{-6} bar and $P_{H2} \approx 9.2 \times 10^{-6}$ bar will be found. However, even these small equilibrium concentrations are sufficient to extract oxygen through an oxygen-selective perovskite membrane.

p0075 Early studies demonstrated the possibility of hydrogen production from direct water decomposition using the mixed-conducting oxygen-selective membrane at extremely high temperatures of 1400–1800 °C. Balachandran et al. [53] fed hydrogen on the permeation side to consume the permeated oxygen. In this case, a high oxygen partial pressure gradient across the membrane was established, and a high hydrogen production rate of $6\,cm^3\,min^{-1}\,cm^{-2}$ at 900 °C was obtained. An even higher hydrogen production rate of $10\,cm^3\,min^{-1}\,cm^{-2}$ could be achieved by using Gd-doped CeO_2 as mixed-conducting membrane with an optimized microstructure [54]. However, hydrogen production by consuming the oxygen on the permeate side, using externally produced hydrogen, may represent a proof of principle, which is, of course, impractical. When methane is used to consume the permeated oxygen by partial oxidation of methane (POM) according to $CH_4 + \frac{1}{2}O_2 \rightarrow CO + 2\,H_2$, not only the oxygen permeation rate can be increased due to the higher oxygen partial pressure gradient across the membrane, but it is also possible to obtain synthesis gas (a mixture of carbon monoxide, CO, and hydrogen, H_2), which can be used to synthesize a wide variety of valuable hydrocarbons (diesel) or oxygenates (methanol), or which can be transformed at lower temperature as well into hydrogen by the water-gas shift reaction according to $CO + H_2O \rightarrow H_2 + CO_2$.

p0080 **Figure 4** presents the concept of the simultaneous production of hydrogen and synthesis gas in a BCFZ
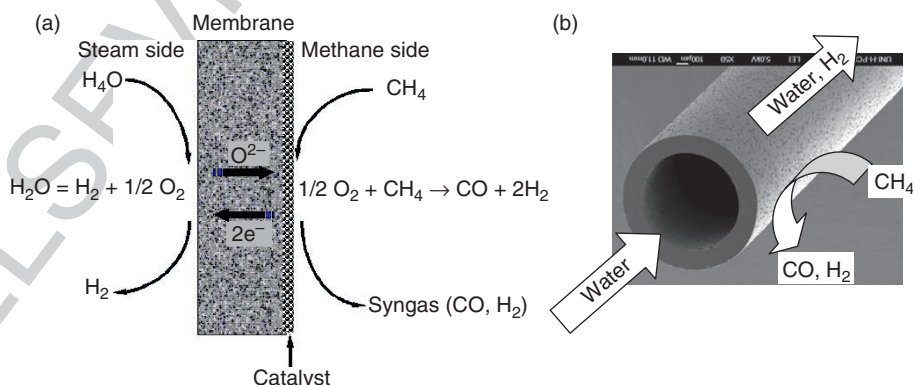
f0020 **Figure 4** The concept of simultaneous production of hydrogen and synthesis gas by combining water splitting and partial oxidation of methane (POM): (a) reaction mechanism and (b) its realization in a perovskite oxygen-permeable hollow-fiber membrane.

perovskite hollow-fiber membrane reactor. At temperatures of 800–900 °C, water is sent to the steam/core side of the BCFZ hollow fiber and, at these temperatures, water starts to dissociate into hydrogen and oxygen. When the oxygen partial pressure on the core/steam side of the BCFZ hollow fiber is higher than that on the shell/methane side, oxygen permeates from the steam/core side to the methane/shell side, where oxygen is quickly consumed by the POM. Thus, oxygen and hydrogen become separated, and the water splitting can continue. Obviously, the hydrogen production rate directly depends on the rate of oxygen removal from the water dissociation system. As shown in **Figure 4**, a high hydrogen production rate of about $2.25 \, cm^3 \, min^{-1} \, cm^{-2}$ at 900 °C is obtained.

p0085   We can learn from **Figure 5** that the hydrogen production rate increases as the temperature rises from 800 to 950 °C and a hydrogen flux of $3.1 \, cm^3 \, min^{-1} \, cm^{-2}$ was obtained at 950 °C [52]. When the temperature is increased, the equilibrium constant of the endothermic water splitting will increase according to the van't Hoff equation. Therefore, the equilibrium is shifted toward the water dissociation and more hydrogen can be produced. Moreover, with increasing temperature, both the rate of the POM and the permeability of the BCFZ hollow-fiber membrane will increase. So, the hydrogen production rate becomes higher with rising temperature.

p0090   In fact, not only hydrogen is produced as retentate on the steam/core side of the BCFZ hollow-fiber membrane after water condensation, but also synthesis gas (CO and H_2) can be simultaneously produced on the methane/shell side. The exit gas of the

methane/shell side mainly consists of H_2, CO, and small amounts of CO_2, H_2O, and unreacted methane. According to previous studies [79, 81], the so-called POM process using a Ni-based catalyst is first a total oxidation followed by steam and CO_2 reforming. However, the products of total oxidation (CO_2 and H_2O) can be transformed with a fine-tuned amount of unreacted methane by catalytic steam- and dry-reforming steps to synthesis gas.

3.01.3 Selectivity Enhancement in Distributor/Contactor-Type Membrane Reactors Operating under Reaction Kinetics Conditions

3.01.3.1 Partial Oxidation of Hydrocarbons by Nonselective Supply of Oxygen through a Porous Membrane as Reactor Wall

Pore membranes can be used for the nonselective feeding of air or oxygen through membranes, thus providing a low and uniform oxygen partial pressure along the axial dimension of a tube reactor [2, 9]. Because of the slight differences of the kinetic diameters of oxygen (0.344 nm) and nitrogen (0.364 nm), the air dosing is usually not combined with an oxygen enrichment. The concept is based on the different dependencies of the rates of partial and total oxidation (hydrogenation), respectively, on the concentration of oxygen (hydrogen). If the reaction rate is described by a power law, the exponent of the oxygen (hydrogen) concentration in the rate equation is higher for total oxidation (hydrogenation) than that for partial oxidation (hydrogenation).
p0095
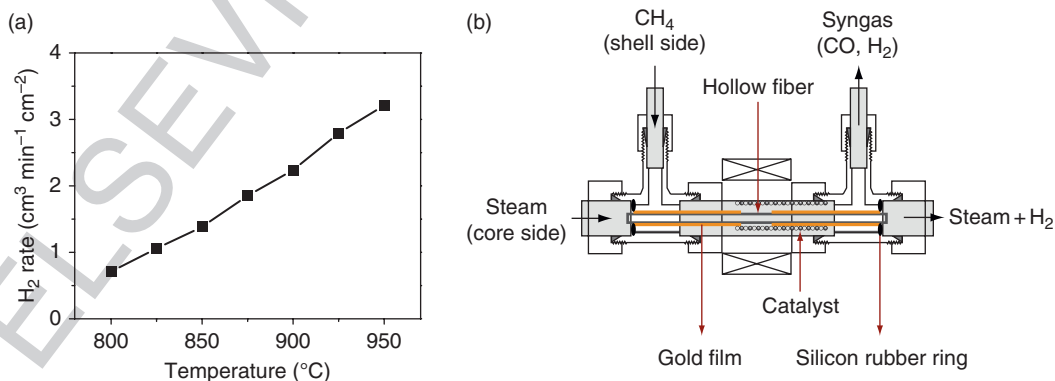
Figure 5 H_2 production by water splitting: (a) hydrogen generation on the core/steam side as a function of temperature [52]; and (b) the experimental setup. Core/steam side: $F_{H2O} = 30 \, cm^3 \, min^{-1}$ and $F_{He} = 10 \, cm^3 \, min^{-1}$. Shell/methane side: $50 \, cm^3 \, min^{-1}$ ($F_{He} = 45 \, cm^3 \, min^{-1}$, $F_{Ne} = 3 \, cm^3 \, min^{-1}$, and $F_{CH4} = 2 \, cm^3 \, min^{-1}$). Amount of packed Ni/Al_2O_3 catalyst: 0.8 g. Effective membrane area: $0.89 \, cm^2$.

A low oxygen (hydrogen) partial pressure along the reactor should be beneficial, therefore, for a high oxygenate (hydrogenate) selectivity.

p0100   In the oxidative dehydrogenation of ethane (ODE), the selectivity and yield for ethylene were found to increase by $\approx$10% if air is dosed continuously along a porous tube reactor [16]. A similar improvement of the selectivity of 8–10% compared to a conventional packed bed reactor at equal conversions was found for the oxidative dehydrogenation of propane (ODP) [55].

p0105   In the case of the maleic acid (MA) anhydride synthesis by n-butane partial oxidation on vanadium phosphorous oxide (VPO), reactor simulations did forecast improved selectivities by oxygen distribution along the length axis of the tube reactor [56]; however, in the experiments, only a modest improvement of selectivity was found [57]. Due to a low oxygen/n-butane ratio at the reactor inlet, the vanadium catalyst was in a reduced state. With increasing conversion of n-butane, the oxygen/n-butane ratio increased and the V^{5+} species responsible for the MA selectivity were formed. However, by doping the VPO catalyst with Co or Mo, the active V^{5+} species could be stabilized even at the low oxygen/n-butane ratio of 0.6 [58].

p0110   As a last example for improved selectivities in partial oxidations when the oxygen is fed into the reactor through a porous wall, the direct oxidation of propane to acrolein is addressed. Acrolein selectivities which were two- to fourfold higher than those in the classical co-feed reactor were obtained at equal propane conversion (**Figure 6**) [59].

3.01.3.2   POM to Synthesis Gas in a Perovskite Hollow-Fiber Membrane Reactor

In Section 3.01.3.1, the nonselective dosing through the porous reactor wall was taken to control the partial pressure of a gaseous reactant over the reactor, whereas, here, the selective dosing of oxygen from air through a highly oxygen-selective perovskite membrane is discussed.

p0115

    An attractive route for the utilization of natural gas is its conversion to synthesis gas ($CO + H_2$). Up to now, the strongly endothermic steam reforming (StR) is the dominant process for producing syngas from natural gas giving a H_2/CO ratio of 3, which is unsuitable for methanol or Fischer–Tropsch synthesis. Therefore, the slightly exothermic POM to syngas, which gives a H_2/CO ratio of 2, has drawn much attention. Although POM with air as the oxygen source is a potential alternative to StR, the downstream requirements cannot tolerate the presence of nitrogen. Therefore, pure oxygen is required, and a significant part of the investment costs associated with conventional POM to syngas is those of the oxygen separation plant. In comparison with StR, the catalytic POM is estimated to offer cost reductions of about 30% [60]. Dense mixed oxygen-ion- and electron-conducting membranes are selectively permeable to oxygen at high temperatures between 800 and 900 °C. Thus, from air only the oxygen ions can be transported through the membrane to the reaction side, where it reacts with the methane to syngas. Local charge neutrality is
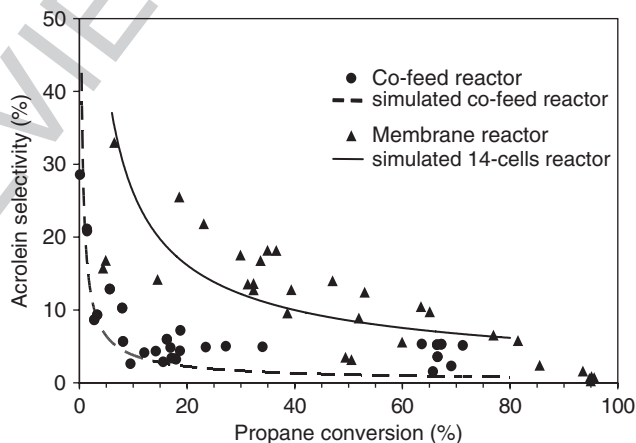
p0120

Figure 6   Direct partial oxidation of propane to acrolein in a conventional co-feed reactor and in a membrane reactor with oxygen dosage through a porous membrane [59]: experimental data and simulation of the acrolein selectivity as a function of the propane conversion. The bifunctional catalyst $Ag_{0.01}Bi_{0.85}V_{0.54}Mo_{0.45}O_4$ was deposited as layer direct on the porous wall of the reactor.

maintained by the counter-current transport of electrons. No external electrodes and electricity are needed and cheap air can be used as oxygen source for POM; the pure oxygen separation and the POM reaction are combined in one reactor and hot spots, as in the conventional co-feed reactor, can be eliminated due to the gradual feeding of oxygen through the membrane.

p0125   So far, mainly relatively thick disk-shaped membranes with a limited membrane area were studied because disks can be easily fabricated by a conventional pressing method. Although a multiple planar stack can be adopted to enlarge the membrane area to an industry-relevant scale, many problems, such as the high-temperature sealing and the pressure resistance, have to be faced [61]. Tubular membranes with diameters in the centimeter range with thick walls were developed to reduce the engineering difficulties, especially the problems associated with the high-temperature sealing [62]. However, their small surface-area-to-volume ratio and their relatively thick walls lead to a low oxygen flux and make them unfavorable in practice. A membrane with a thin wall in a hollow-fiber geometry can solve the problems mentioned above. Compared to the disk and tubular membranes, hollow-fiber membranes possess much larger membrane area per unit volume for oxygen permeation [63, 64]. Furthermore, the resistance of the hollow-fiber membrane as a full material (i.e., nonsupported) to oxygen permeation is very much reduced due to the thin wall as it is the case for supported thin perovskite films. Other model solutions are multichannel monoliths, tube-and-plate assemblies, or single-hole tubes. Praxair has developed about 2-m-long single-hole tubes prepared by extrusion [65]. The so-called tube-and-plate concept of Air Products consists of $10 \, cm \times 10 \, cm$ plates connected with a central support tube for the pure oxygen [66–68]. Hydro Oil and Energy developed a multichannel monolith for oxygen separation [69]. Whereas the industrial realization of a catalytic membrane reactor is still an aim that is difficult to realize, the implementation of a perovskite-based plant for the production of oxygen-enriched air or of air separation seems to be easier feasible. By Vente et al. [70] the membrane geometries of single-hole tubes, multichannel monoliths, and hollow fibers for air separation are evaluated.

p0130   Looking back, the breakthrough in the wide application of membranes in dialysis, natural gas and refinery gas treatment is closely linked to the development of organic hollow fibers spun from organic polymers. Therefore, there are increasing activities to prepare inorganic hollow fibers, including gas-tight perovskite hollow fibers for oxygen transport at elevated temperatures (e.g., References 71–74). Recently, from the modified perovskite composition BCFZ ($x + y + z = 1.0$) [75], O_2-permeable hollow-fiber membranes, with high O_2 permeation flux and excellent thermal and mechanical properties, have been prepared [76–78]. **Figure 7(a)** schematically shows a hollow-fiber membrane reactor; **Figure 7(b)** demonstrates the experimental setup. Two ends of the hollow fiber were sealed by Au paste and placed in a gas-tight dense alumina tube. Therefore, such an Au-sealed short piece of a hollow-fiber membrane can be kept in the middle of the oven, thus ensuring real isothermal conditions.

In the POM to synthesis gas, the optimization of a p0135 laboratory-scale reactor as shown in **Figure 7** using BCFZ hollow-fiber membranes [76] gave CO selectivities of $S(CO) = 96\%$ for methane conversions $X(CH_4) = 95\%$ if the commercial Ni-based StR catalyst (Süd-Chemie) is placed around and behind the perovskite hollow fiber (seen from reactor inlet to the outlet direction) (**Figure 8**). The BCFZ hollow-fiber membrane reactor could be operated up to 300 h in the POM without failure [17]. Air, as the oxygen source, was passed through the tube side of the fiber; methane and the catalyst were outside. Knowing that the mechanism of the POM cannot be stopped at the intermediates CO and H_2, this reaction can be viewed as a total oxidation followed by the so-called dry and steam reforming of the total oxidation products CO_2 and H_2O by CH_4 [79]. Therefore, the above-mentioned StR catalyst was used. However, two problems had to be solved: (1) coke deposition occurs and results in a mechanical blocking of the reactor after about 50 h time on stream. By using methane/steam mixtures as the feed with $CH_4/H_2O \leq 1$, coke deposition could be completely avoided. (2) The BCFZ hollow fiber was destructed by $BaCO_3$ formation in the cold region of the reactor near to the reactor outlet at about 600 °C. Since CO_2 formation cannot be avoided completely, carbonate formation had to be stopped for thermodynamic reasons by having the whole perovskite fiber at 875 °C. This required a novel hot sealing technique for short pieces of a hollow fiber by using Au paste (**Figure 7(b)**). As a result, the laboratory-scale reactor could be operated several hundred hours in the POM (**Figure 9**).

Figure 10 represents the possible pathways in the p0140 POM showing an interplay of total and partial
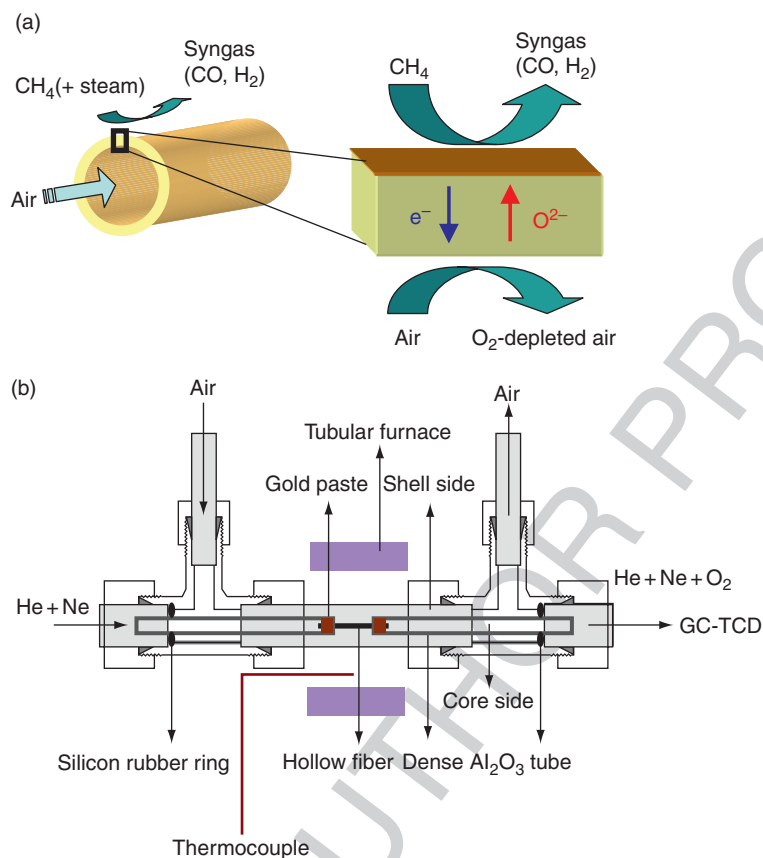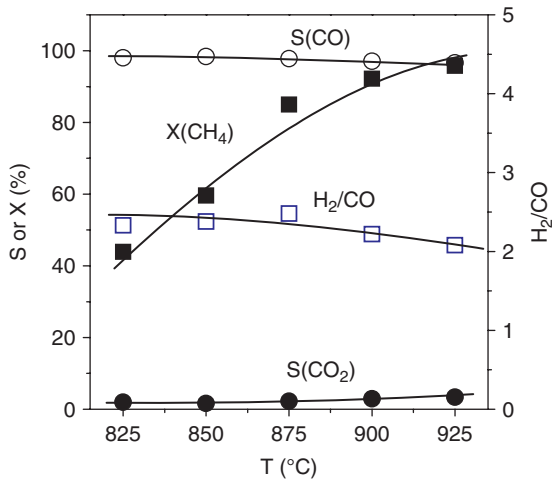
Figure 7   Partial oxidation of methane (POM) to synthesis gas: (a) scheme of the POM reaction with oxygen separated from air. Air is sent through the core side of the perovskite hollow-fiber membrane; oxygen is transported through the mixed ion and electron-conducting membrane to the shell side where the catalytic partial and total oxidations of methane followed by steam reforming and dry reforming take place [17]. (b) The one hollow-fiber catalytic membrane reactor using gold paste for the hot sealing of the fiber. Effective fiber length: 11.9 mm, outer diameter: 0.88 mm, inner diameter: 0.52 mm [17].

oxidations as well as reforming reactions as it was proposed by Kondratenko and Baerns [80]. We could obtain high methane conversions and high CO selectivities only, when some Ni-based StR catalyst was packed behind the oxygen permeation zone (zone 3 in **Figure 8**) where the reforming of the total oxidation products, CO_2 and H_2O, with unreacted CH_4 can take place. Consequently, the synthesis gas formation from methane in a mixed-conducting perovskite membrane reactor is called an oxidation-reforming process [79, 81].

p0145   Perovskite hollow-fiber membranes were successfully tested over several hundred hours in the POM to synthesis gas (typical product gas composition 65% H_2, 31% CO, 2.5% unreacted CH_4, and 1.5% CO_2) and the production of oxygen-enriched air (O_2 content between 30% and 45%). When arranged in bundles, hollow fibers can reach high membrane area per reactor/permeator volume. Economic goals, as membrane

area per m^3 permeator volume of the order of 5000 $m^2 m^{-3}$ at a price of about 1000 € m^{-2} noninstalled area, are met by the perovskite hollow fibers. Based on our results, the amount of oxygen necessary for a methanol plant with a capacity of 2000 tons day^{-1} based on POM could be delivered by 4 600 000 hollow fibers. Assuming a fiber length of 1 m, this would lead – depending on the packing – to a cylindrical module of only 4-m diameter.

p0150   It should be noted that mixed-oxygen-ion- and electron-conducting membranes in hollow-fiber geometry have been successfully tested not only for the syngas production but also for the preparation of oxygen-enriched air [82, 83], the oxi-dehydrogenation of hydrocarbons to the corresponding olefins [84], and the oxidative coupling of methane (OCM) to C_{2+} hydrocarbons. These processes are discussed in the following section.

Figure 8 CH$_4$ conversion, CO and CO$_2$ selectivities, as well as H$_2$/CO ratio of the BaCo$_x$Fe$_y$Zr$_z$O$_{3-\delta}$ (BCFZ) perovskite hollow fiber used as membrane reactor in the partial oxidation of methane (POM) reaction as a function of temperature. To avoid coking, the feed contained 8.4 vol.% steam [17].

3.01.3.3 Hydrocarbon Partial Oxidation with Selective Oxygen Supply

Oxidative ODE and ODP to the respective olefins is considered as a promising alternative to the (catalytic) thermal dehydrogenation, since there is no equilibrium constraint on the conversion. However, the yields attained so far in the oxidative dehydrogen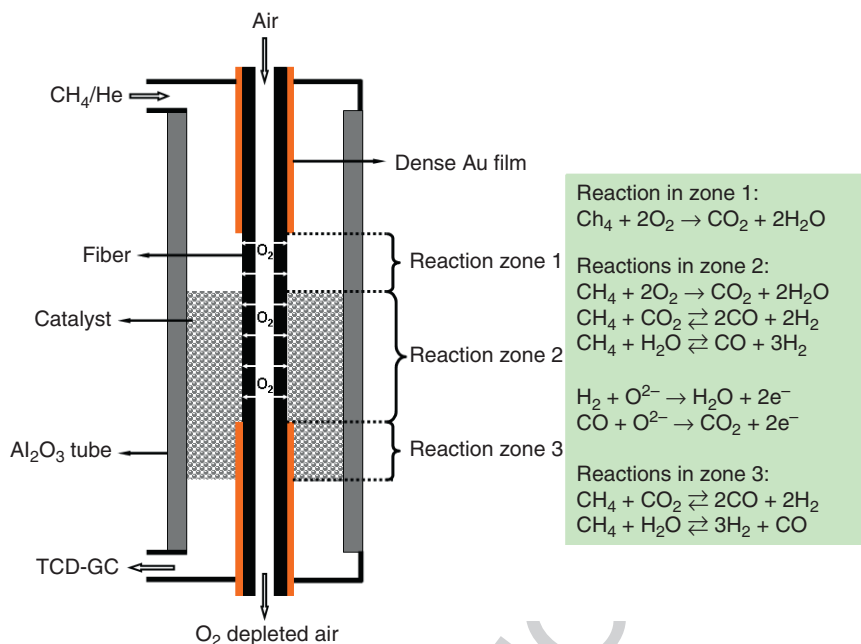ations in conventional co-feed reactors are too low for an industrial application. However, during the past few years, remarkable progress could be observed in the classical co-feed ODE, especially by reaction engineering measures, leading to ethene yields up to 56% at 71% selectivity in autothermal oxidative dehydrogenation at short contact time of ~45 ms, using catalysts as igniters [85]. A high propene yield of 30% was obtained on K-Mo catalysts on SiO$_2$–TiO$_2$ supports using a diluted feed (92.5% inert, 5% propane, and 2.5% O$_2$) [86]. Propene yields of 22% are reported on intercalated Mo catalysts also for diluted feeds (73% inerts, 18% propane, and 9% O$_2$) [87]. A reasonable propene yield of 18% with an excellent space time yield of 12 kg propene kg^{-1} h^{-1} was obtained for VO$_x$ on MCM-48 [88].

First results on oxidative dehydrogenations using oxygen-transporting membranes showed superior yields compared to classical co-feed fixed-bed reactors. In ODE using planar and tubular oxygen-conducting membranes from Ba$_{0.5}$Sr$_{0.5}$Co$_{0.8}$Fe$_{0.2}$O$_{3-\delta}$ an ethene selectivity of 80% at 84% conversion was found at 800 °C [89, 90]. The same material reached 66% ethene yield at 807 °C, which could be further increased to 76% at 777 °C by incorporation of Pd clusters [91, 92]. An ethene yield of 56% per pass, together with an ethene selectivity of 80%, was achieved in a dense tubular ceramic membrane reactor made of Bi$_{1.5}$Y$_{0.3}$SmO$_3$ at 875 °C [93].

Compared to ODE, there are only a few papers on ODP in mixed ion–electron-conducting (MIEC)
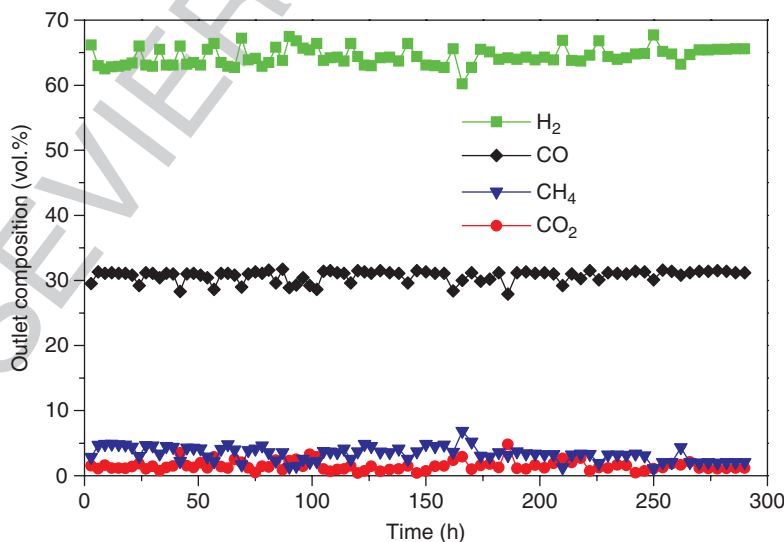
Figure 9 Off-gas composition in the partial oxidation of methane (POM) reaction. The gas composition 65% H$_2$, 31% CO, 2.5% CH$_4$, and 1.5% CO$_2$ corresponds to X(CH$_4$) = 95%, S(CO) = 96%, and S(CO$_2$) = 4%, feed = CH$_4$ with 55 ml min^{-1} + H$_2$O with 5 ml min^{-1}, temperature = 875 °C; pressures on both sides of the BaCo$_x$Fe$_y$Zr$_z$O$_{3-\delta}$ (BCFZ) hollow-fiber membrane: 1 bar [17].

Air

CH$_4$/He

Dense Au film

Fiber

Catalyst

Al$_2$O$_3$ tube

TCD-GC

O$_2$ depleted air

Reaction zone 1
Reaction zone 2
Reaction zone 3

Reaction in zone 1:
Ch$_4$ + 2O$_2$ → CO$_2$ + 2H$_2$O

Reactions in zone 2:
CH$_4$ + 2O$_2$ → CO$_2$ + 2H$_2$O
CH$_4$ + CO$_2$ ⇄ 2CO + 2H$_2$
CH$_4$ + H$_2$O ⇄ CO + 3H$_2$

H$_2$ + O^{2-} → H$_2$O + 2e$^-$
CO + O^{2-} → CO$_2$ + 2e$^-$

Reactions in zone 3:
CH$_4$ + CO$_2$ ⇄ 2CO + 2H$_2$
CH$_4$ + H$_2$O ⇄ 3H$_2$ + CO

Figure 10 Reaction pathways in the catalytic perovskite hollow-fiber membrane reactor [81]. Note that the Ni catalyst can be in different redox states according to the surrounding gas phase: In zone 1, the catalyst is present mainly as NiAl$_2$O$_4$; in zone 2, as NiO/Al$_2$O$_3$; and in zone 3, as Ni/Al$_2$O$_3$.

membrane reactors. Using a Ba$_{0.5}$Sr$_{0.5}$Co$_{0.8}$Fe$_{0.2}$O$_{3-\delta}$ perovskite and a diluted feed (90% inert and 10% propane), propene selectivities of 44.2% were found [94]; at low propane conversion (5%), the propene selectivity was 52%. These results show that – in contrast to ODE – there is no improvement for ODP, as yet, in using oxygen-transporting membrane; the performances reported are still below those of classical co-feed fixed-bed reactors.

Because of the high temperatures in the perovskite membrane reactors for the ODE and ODP, an overlap of the desired oxidative dehydrogenation with the noncatalytic gas-phase dehydrogenation, including cracking, coking, and other high-temperature reactions, takes place [84]. The performance of MIEC membrane reactors depends on membrane geometry as well: for ODE using Ba(Co,Fe,Zr)O$_{3-\delta}$ membranes with a disk geometry almost 80% selectivity to ethene was observed, whereas hollow-fiber membranes reached only 40% (**Figure 11** and **Table 3**). This was explained by the different contact times in the two reactor configurations, that is, with hollow-fiber membrane, deep oxidation of ethene to CO and CO$_2$ could not be avoided. Once ethene is formed, it reacts again with lattice oxygen or gaseous oxygen to form CO$_x$ and H$_2$O.
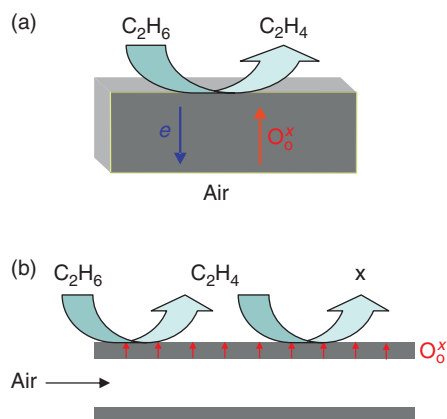
Figure 11 Comparison of the oxidative dehydrogenation of ethane (ODE) in the oxygen-transporting disk membrane reactor (a) and in the hollow-fiber membrane reactor (b) [84]. For the results see **Table 3**.

Similar to ODE and ODP, the OCM to C$_2$ hydrocarbons (ethane and ethene) is a widely studied topic in C$_1$ chemistry. Methane activation for OCM by lattice oxygen from an MIEC membrane looks promising as well (**Figure 12**). However, the high-temperature level where the oxygen-transporting membranes work implies that side reactions, such as

Table 3 Oxidative dehydrogenation of ethane to ethylene according to $C_2H_6 + 1/2\ O_2 \rightarrow C_2H_4 + H_2O$ (see **Figure 11**)

Reactor types	Membrane surface area (cm²)	C₂H₆ conversion (%)	Product selectivity (%)			
			C₂H₄	CH₄	CO	CO₂
Disk membrane	0.9	85.2	79.1	10.7	5.4	4.8
Hollow fiber	3.52	89.6	39.9	12.1	15.4	32.6

Comparison between a $Ba(Co,Fe,Zr)O_{3-\delta}$ perovskite disk and a hollow-fiber membrane reactors at 850 °C. Feed: $40\ ml_N\ min^{-1}$, Ethane diluted with 90% He on the core side; air flow rate on the shell side: $300\ ml_N\ min^{-1}$ [84].
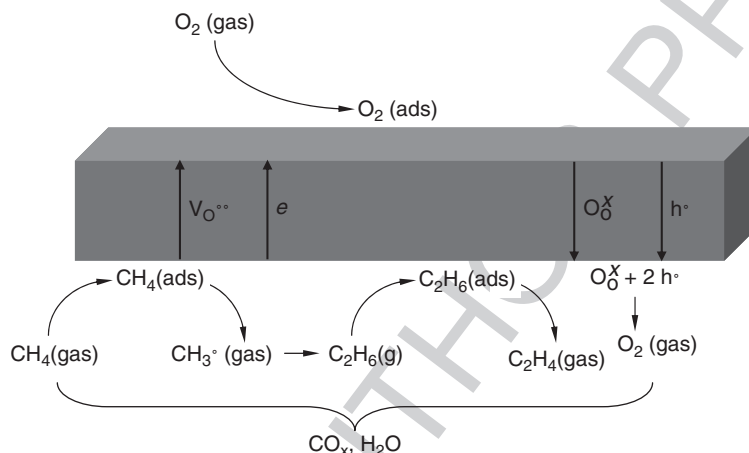
Figure 12 Possible mechanisms of the oxidative coupling of methane (OCM) in an oxygen-transporting membrane reactor [94].

thermal cracking and a variety of radical reactions, occur. Most probably, in oxygen-transporting membrane reactors (1) direct POM at the perovskite surface, (2) formation of radicals at the perovskite and/or catalyst surface, and (3) radical reactions both at the catalyst surface and in the gas phase occur simultaneously. Therefore, solid catalysts were proposed to support the OCM reaction. One of the highest C_2 yields, that is, 35% at a C_2 selectivity of 54%, was obtained in a tubular membrane reactor with a $Bi_{1.5}Y_{0.3}Sm_{0.2}O_{3-\delta}$ MIEC membrane [95]. However, the feed was strongly diluted (2% CH_4 in He): $BaSrCoFe\ O_{3-\delta}$ [96] and $BaCeGdO_{3-\delta}$ [97] of different chemical compositions. Typical results are C_2 selectivities of 70–90% for methane conversions below 10% and diluted feeds. If the CH_4 content in the feed is increased, the C_2 selectivity drops below 40%.

p0180   On the one hand, the direct supply of oxygen from air through an oxygen-transporting membrane for ODE, ODP, and OCM seems to be very promising. On the other hand, the high temperatures of 800–900 °C, usually applied to achieve sufficient high oxygen flux, spoil the selectivity of these reactions.

There are recent attempts to develop oxygen-transporting materials with sufficient oxygen flux at low temperatures, such as 500–600 °C. As an example, **Figure 13** shows the oxygen fluxes through a BCFZ hollow-fiber perovskite membrane. **Figure 13**(**a**) shows the low-temperature oxygen fluxes through a BCFZ hollow-fiber membrane after 20 min time on stream. As **Figure 13**(**b**) shows, the oxygen fluxes decrease with permeation time but the initial oxygen-transport characteristics can be restored after a 1-h treatment of the spent BCFZ hollow-fiber membranes at 925 °C in air [98].

3.01.3.4 *p*-Xylene Oxidation to Terephthalic Acid in a Reactor with a Bifunctional Membrane
s0055

There are ambitious attempts to combine membrane p0185 layers of different functionality. As a first example, for shape-selective oxidations, a thin Ti-doped silicalite-1 layer was crystallized on a BCFZ oxygen-transporting perovskite membrane in disk geometry [100]. If a mixture of the xylene isomers would be in
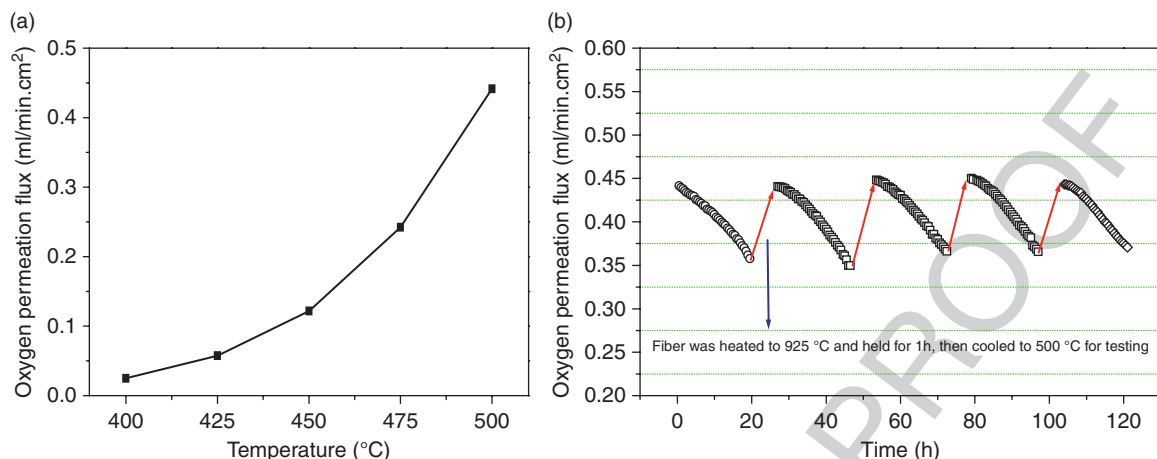
f0065　**Figure 13**　Low-temperature oxygen permeation (flow rate: 150 ml min^{-1} air on the shell side, 30 ml min^{-1} He on the core side; 0.43 cm^2 effective membrane area) [98]: (a) oxygen permeation flux through a BaCo$_x$Fe$_y$Zr$_z$O$_{3-\delta}$ (BCFZ) hollow-fiber membrane as a function of temperature, and (b) oxygen permeation fluxes through a BCFZ hollow-fiber membrane as a function of time at 500 °C (flow rate: 150 ml min^{-1} air on the shell side, 30 ml min^{-1} He on the core side; the effective area of hollow-fiber membrane: 0.43 cm^2).

contact with this bilayer membrane facing the Ti-modified silicalite-1 layer, it can be expected that mainly the *p*-xylene isomer will enter the silicalite-1 layer and will become oxidized to the terephthalic acid with the oxygen released from the perovskite membrane. As **Figure 14** shows, this concept works indeed. From a technical C$_8$ stream, it is the *p*-xylene, indeed, that has been partially oxidized to terephthalic acid.

s0060　### 3.01.3.5　Partial Hydrogenation of Cyclooctadiene to Cyclooctene in a Pore-through-Flow Membrane Reactor

p0190　The partial hydrogenation of a di-olefine to the corresponding monoolefine represents a consecutive reaction of the type A → B → C. The pore-through-flow membrane reactor, as a special type of a membrane contactor, was used for the partial hydrogenation of 1,5-cyclooctadiene (COD) to cyclooctene (COE) (**Figure 15**). A catalytic membrane contactor is a device in which a membrane containing a catalytically active phase is used to provide the reaction zone, thereby the membrane not necessarily has a separative function. In the selective hydrogenation of COD to COE, we have the case of a reaction network of the type $A \xrightarrow{+H_2} B \xrightarrow{+H_2} C$, where the consecutive reaction of the desired intermediate B to C should be avoided. In fixed-bed reactor with catalyst pellets, the selectivity of such reactions is limited by mass transport
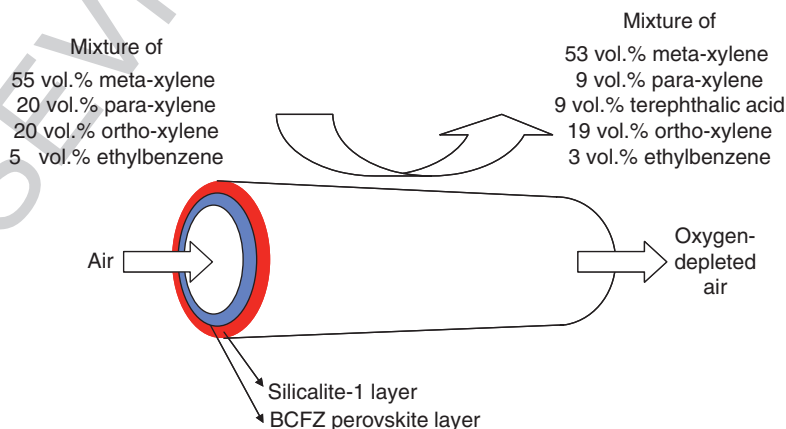
f0070　**Figure 14**　Partial oxidation of *p*-xylene from a technical C$_8$ mixture to terephthalic acid in a bilayer BaCo$_x$Fe$_y$Zr$_z$O$_{3-\delta}$ (BCFZ)/Ti-silicalite-1 membrane reactor at 850 °C [100].
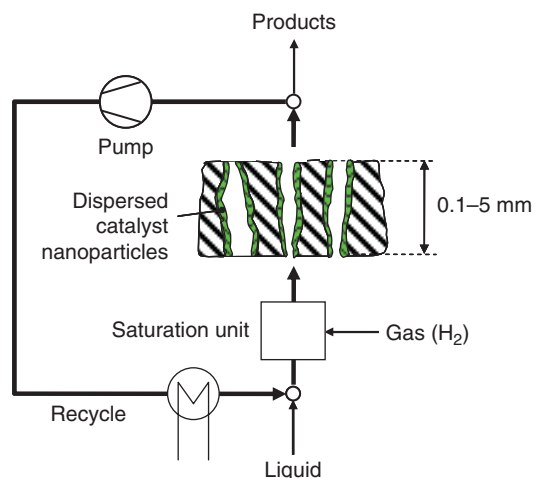
Figure 15   Schema of the pore-through-flow catalytic membrane reactor for hydrogenations of multi-unsaturated hydrocarbons as a special case of a catalytic membrane contactor reactor: the Pd catalyst is placed on the pore walls over the whole cross section of a symmetric membrane. In every loop, the feed becomes H_2-saturated again [2].

due to diffusion processes into and out of the pores of the catalyst. This pore diffusion increases the contact time of the intermediate B at the catalytically active sites, which promotes the formation of C. In the pore-through-flow membrane reactor, the selectivity limitation by diffusion can be avoided because the reactants pass the membrane in a fast convective flow. As a consequence, higher activity and increased selectivity to the intermediate product C can be expected. By applying a high flow rate, this operation mode allows one to eliminate the influence of the

diffusional resistance present in conventional porous catalysts, thus offering the perspective to exploit the true kinetic properties of the solid active phase, that is, higher activity and improved selectivity in consecutive reactions. The catalytically functionalized pores of the membrane provide a medium with defined contact times for the co-feed of hydrogen and an unsaturated hydrocarbon. Applications of membranes with built-in catalysts for gas/liquid reactions have been reviewed by Dittmeyer *et al.* [101].

A number of authors have investigated membrane p0195 contactors to improve the performance of gas/liquid reactions, mainly of hydrogenations. Several groups studied the selective hydrogenation of nitrate and nitrite in water to nitrogen on bimetallic Pd/Cu- and Pd/Sn- or monometallic Pd catalysts, which were either directly deposited into porous ceramic membranes [102–104] or embedded as alumina-supported powder catalysts in porous polymer membranes. Others tested the pore-through-flow concept for the selective hydrogenation of edible oils [105] and of various unsaturated organic substrates, such as 1-octyne to octene, phenylacetylene to styrene, COD to COE, and geraniol to citronellol [106].

The porous alumina membranes were deposited p0200 with Pd by wet impregnation with a Pd salt solution and subsequent activation by a reducing agent. Their catalytic activity and selectivity were investigated in a reactor system constructed as a loop of a saturation vessel and a membrane module for the partial hydrogenation of COD to COE (see **Figure 16**). Details about impregnation procedure and experimental setup are given by Schomäcker *et al.* [107]. The
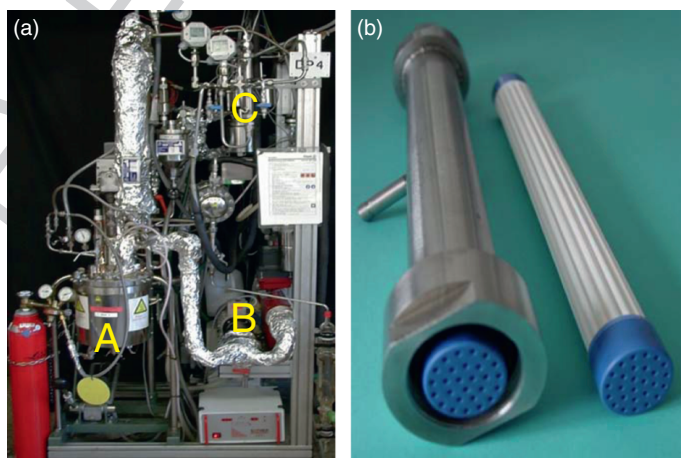
Figure 16   Pilot-scale loop membrane contactor reactor for the selective hydrogenation working due to the pore-through-flow principle (a) and the porous 27-tube ceramic module used in the scale-up (b). A: saturation unit, B: circulation pump, C: membrane module [17].

hydrogenation reactions were transferred from laboratory to the pilot scale at Bayer Technology Services GmbH. The volume of the saturation unit was increased from 0.2 to 5.2 l and the membrane area from 20 to 500 cm^2. The flow rate of the reaction mixture per membrane area was kept constant. The loop reactor is shown in **Figure 16**(**a**). The 27-tube membrane module used is shown in **Figure 16**(**b**). The functionalization of the ceramic tubes by Pd particles was done according to the same procedure that was used for single membrane tubes. The COD hydrogenation experiments were performed in a range of 30–60 °C, 0.1–1 MPa hydrogen pressure, and 0.5–2 kg m^{-2} s^{-1} circulation flow rates and using membrane tubes with a pore diameter of 0.6–3.0 μm. Both in the laboratory as well as in the pilot scale, the same loop reactor, the scheme of which is shown in **Figure 15**, was used. The H$_2$-saturated liquid is pumped as feed at high flow rates through the membrane, thus eliminating the diffusive mass transfer resistance.

p0205   For the partial hydrogenation of COD, the selectivity for COE is higher in the pore-through-flow membrane reactor compared to a fixed-bed reactor or a slurry reactor with catalyst pellets (**Figure 17**). The highest COE selectivity (95% at complete conversion) is obtained in a slurry reactor with a suspended powder catalyst, because all mass transfer limitations are avoided here. The same result is obtained in the pore-through-flow membrane reactor, indicating that the hydrogenation reaction in the pore-through-flow membrane reactor is indeed only controlled by the microkinetics of the reaction and not by mass transfer effects, such as pore diffusion (**Table 4**).

p0210   The selective hydrogenation of COD to COE was successfully scaled up to the pilot scale by a factor of 27. This factor was applied to the system volume, membrane area, and circulation flow rate in order to ensure constant reaction conditions. As **Figure 18** shows, the COD conversion and the COE selectivity were comparable in the laboratory-scale apparatus, using a single-tube membrane and in the pilot-scale apparatus using a bundle of 27 membrane tubes. In the pilot plant reactor, the reaction is even somewhat faster than on laboratory scale, while the selectivities
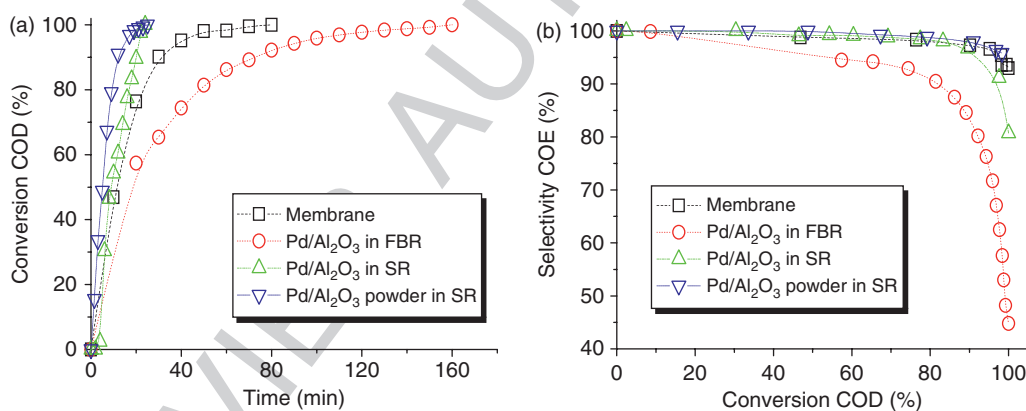
f0085   **Figure 17**   Selectivity improvement when conducting the partial hydrogenation of cyclooctadiene (COD) to cyclooctene (COE) at 50 °C and 1 MPa H$_2$ pressure as a model reaction for a consecutive reaction of the type A → B → C in a pore-through-flow reactor (porous α-alumina membrane; circulation flow rate 120 ml min^{-1} = 0.5 kg m^{-2} s^{-1}) in comparison with a conventional fixed-bed reactor (FBR) and a slurry reactor (SR). Equal amount of 1 mg Pd for all reactors: Pd/Al$_2$O$_3$ (egg-shell type) as 3-mm pellet catalyst with 0.5 wt.% Pd. COD concentration is 0.4 mol l^{-1}: (a) COD conversion vs. time, and (b) COE selectivity vs. COD conversion [17].

t0020   **Table 4**   Selectivities for cyclooctene (COE) in the selective hydrogenation of cyclooctadiene (COD) at complete conversion of COD [17]

Reactor type	Selectivity for COE at X(COD) ≈ 100 %
Pore-through-flow membrane	94%
Slurry (with powder catalyst)	95%
Fixed bed (with shell catalyst)	45%
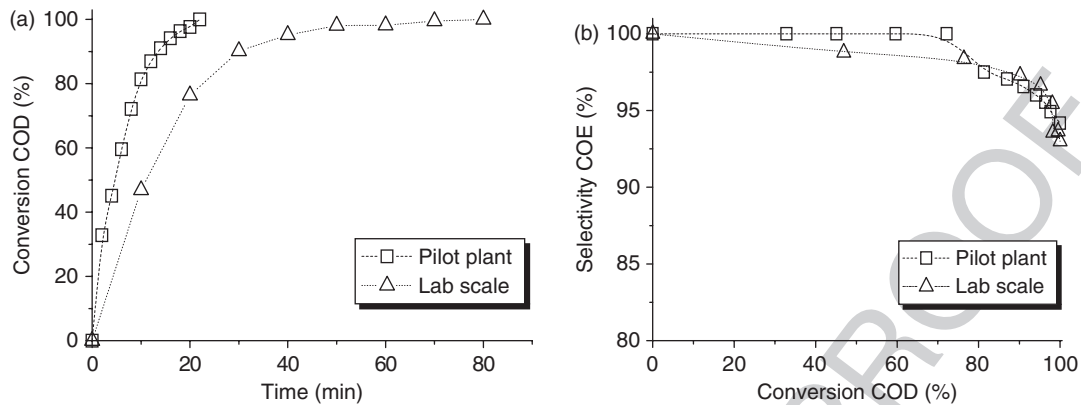
Figure 18   Scale-up of the partial hydrogenation of cyclooctadiene (COD) to cyclooctene (COE) in a pore-through-flow membrane reactor from the laboratory scale to a pilot plant [17, 106], overall volume of lab scale reactor 0.2 l, membrane area 20 cm^2, amount of Pd = 1 mg; overall volume of pilot reactor 5.2 l, membrane area 500 cm^2, amount of Pd = 30 mg. 50 °C, 1 MPa hydrogen pressure, $c_{COD,0} = 0.41$ mol l^{-1}, pore diameter 1.9 μm, and circulation flow rate 0.5 kg m^{-2} s^{-1}: (a) COD conversion vs. time, and (b) COE selectivity vs. COD conversion.

are the same within experimental error. The difference in the rates may be explained by a higher amount of palladium and better dispersion of palladium within the membrane capillary bundle. With these data, a space–time yield for COE of 1 mol l^{-1} h^{-1} and a productivity of 30 mol h^{-1} g$_{palladium}^{-1}$ is obtained. The pore-through-flow membrane reactor used for the partial hydrogenation of a multiunsaturated hydrocarbon was successfully scaled up into the pilot scale. For a process to produce 1 ton h^{-1} of a product by a partial hydrogenation with a similar kinetics than COD hydrogenation, an overall volume of 2–10 m^3 would be required, depending on a suitable reactant concentration. This solution would be circulated through a membrane module with 60 m^2 of porous alumina membrane containing 20 g of palladium. The volume of this membrane module would be below 1 m^3.

3.01.4   Removal of Oxygen as a Reaction Rate Inhibitor in the NO$_x$ Decomposition in an Extractor-Type Membrane Reactor

Nitrous oxide (N$_2$O) has recently received much attention since it greatly contributes to the greenhouse effect and causes a severe destruction of the ozone layer in the stratosphere. N$_2$O is produced by both natural and anthropogenic sources. Compared to the natural sources, N$_2$O emissions, which can be reduced in the short term, are associated with chemical and energy industries. The major N$_2$O emission of chemical production comes from adipic acid and nitric acid plants. In the past few decades, significant efforts have been devoted to the development of technologies for N$_2$O reduction, mainly the selective catalytic reduction (SCR), and the catalytic decomposition of N$_2$O to O$_2$ and N$_2$. The major drawback of the SCR is the high cost associated with the consumption of reductants. Direct catalytic decomposition of N$_2$O without addition of reducing agents is an attractive and economical option to reduce N$_2$O emission. Catalysts, including supported noble metals, metal oxides, and perovskites, have been reported to be active in the direct catalytic N$_2$O decomposition. However, metal-oxide catalysts suffer from oxygen inhibition and a low reaction rate of the N$_2$O decomposition is observed.

The problem of product poisoning in the direct catalytic decomposition of N$_2$O could be solved by *in situ* removal of the inhibitor oxygen, using a perovskite membrane of the composition BCFZ in hollow-fiber geometry [108]. The BCFZ membrane fulfills two tasks: it acts as (1) a catalyst for the decomposition of N$_2$O and (2) a membrane for the removal of the rate-inhibiting surface oxygen. The basic concept is shown in **Figure 19**: N$_2$O catalytically decomposes on the perovskite membrane surface to N$_2$ and surface oxygen (O*) according to N$_2$O → N$_2$ + O* Subsequently, O* is removed as oxygen ions (O^{2-}) through the membrane, while local charge neutrality is maintained by counter-diffusion of electrons (e$^-$). In order to ensure a sufficient driving
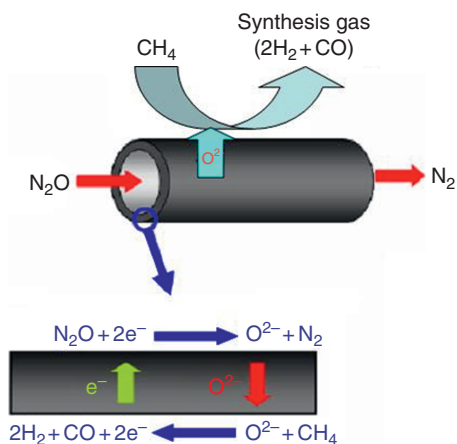
Figure 19   Mechanism of the direct decomposition of N_2O to N_2 with *in situ* removal of the rate-inhibiting surface oxygen by perovskite hollow-fiber membrane [108].

force for the oxygen transport through the membrane, methane is fed to the permeate side of the membrane to consume the permeated oxygen via the POM to synthesis gas according to $CH_4 + O^{2-} \rightarrow CO + 2H_2 + 2e^-$. As a result, surface oxygen (O^*) can be quickly removed by the membrane once it is generated from N_2O decomposition. Therefore, the average amount of adsorbed oxygen (O^*) is reduced and a higher reaction rate of the N_2O decomposition is obtained.

p0225   In order to demonstrate this concept, we carried out experiments with and without oxygen removal using a BCFZ perovskite hollow-fiber membrane. N_2O was fed to the core side and no sweep gas was

applied at the shell side, which means that none of the oxygen surface species produced by the decomposition of N_2O was removed by permeation through the membrane. The corresponding results are shown in **Figure 20**(**a**). The N_2O decomposition increases with increasing temperature; however, the conversion is relatively low (<30% even at 900 °C). The catalytic decomposition of N_2O on the perovskite membrane surface mainly proceeds in two steps: (1) decomposition of N_2O into N_2 and adsorbed surface oxygen (O^*) according to Equation (1) and (2) desorption of surface oxygen as O_2 to the gas phase according to $O^* \rightleftarrows \frac{1}{2}O_2 + ^*$. This reaction, that is, the oxygen–oxygen recombination, is known to be the rate-limiting step in N_2O decomposition [109, 110]. Since the surface oxygen O^* generated by the N_2O decomposition occupies the surface active site for the decomposition of N_2O, only a low N_2O conversion is obtained. Contrary to this poor conversion, if methane as an oxygen-consuming sweep gas is fed to the shell side, the N_2O decomposition is significantly improved as shown in **Figure 20**(**b**).

The membrane approach presented here has to p0230 use a reducing agent, so that it would be sustainable and economically attractive to combine the N_2O removal with the simultaneous production of valuable chemicals. Here, we used the permeated oxygen to produce the N_2-free synthesis gas. **Figure 21** shows the CO selectivity and CH_4 conversion on the shell side as well as the N_2O conversion on the core side as a function of time. N_2O in the core side was completely converted. Simultaneously, synthesis
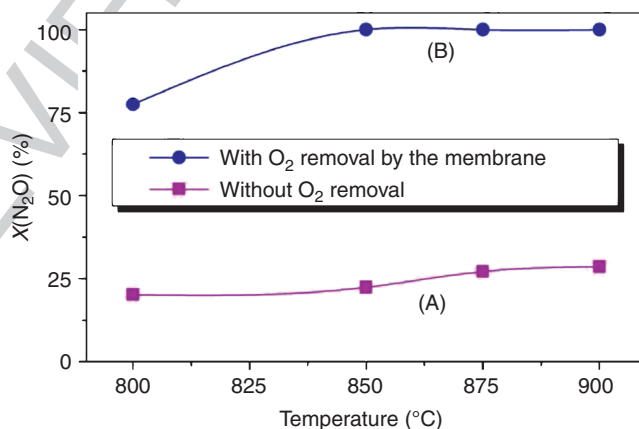
Figure 20   Conversion of N_2O at different temperatures with or without oxygen removal via a perovskite hollow-fiber membrane [108]. Experimental details – core side: 30 cm^3 min^{-1} (F_{N2O} = 6 cm^3 min^{-1}, F_{He} = 24 cm^3 min^{-1}); shell side: (A) no oxygen-consuming sweep gas applied, and (B) with methane as oxygen-consuming sweep gas, 40 cm^3 min^{-1} (F_{CH4} = 8 cm^3 min^{-1}, F_{Ne} = 12 cm^3 min^{-1} and F_{H2O} = 20 cm^3 min^{-1}); membrane area: 0.86 cm^2. Amount of Ni-based catalyst on shell side: 1.2 g.

(a)

(b)
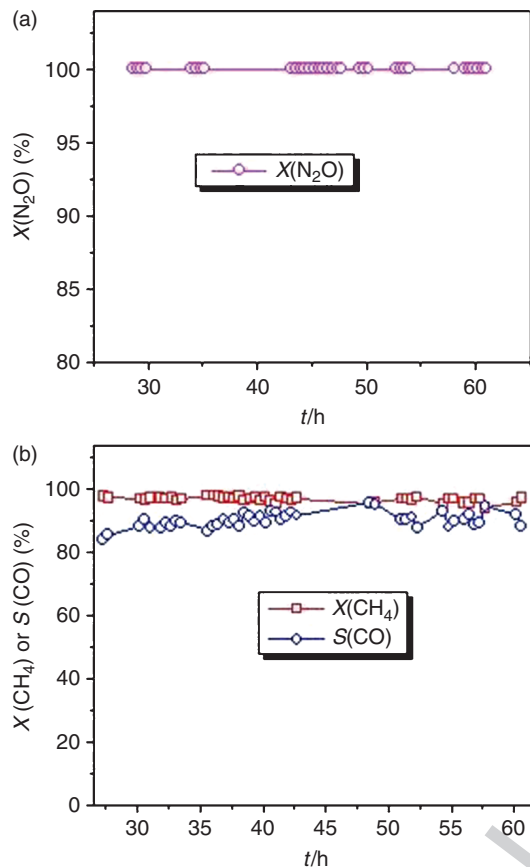
f0105 **Figure 21** N_2O conversion (a), methane conversion and CO selectivity (b) as a function of time on stream at 875 °C [108]. Experimental details – core side: 30 cm^3 min^{-1} ($F_{N2O} = 6$ cm^3 min^{-1}, $F_{O2} = 1.5$ cm^3 min^{-1}, $F_{He} = 22.5$ cm^3 min^{-1}); shell side: 40 cm^3 min^{-1} ($F_{CH4} = 23$ cm^3 min^{-1}, $F_{H2O} = 17$ cm^3 min^{-1}); membrane area: 0.86 cm^2. Amount of Ni-based catalyst on shell side: 1.2 g.

gas is obtained with a methane conversion of 90% and a CO selectivity of 90% for at least 60 h of operation. The technology is more feasible when the concentrations of nitrous oxide in the off-gas are sufficiently high, such as in adipic acid plants.

The same mechanism, similar to that of the N_2O p0235 decomposition, could be successfully applied for the NO splitting into the elements [111]. **Figure 22** [AU7] shows the concept of NO decomposition in the BCFZ perovskite hollow-fiber membrane reactor. First, the adsorbed NO is catalytically decomposed on the surface of the BCFZ membrane into N_2 and surface oxygen (O*), based on the reaction NO $\rightarrow 1/2N_2 + O^*$ [112, 113]. Then, the surface O∗ is removed as oxygen ions (O^{2-}) via the perovskite oxygen-transporting membrane, and local charge neutrality is maintained by the counter-diffusion of electrons (e$^-$). Thus, the surface oxygen (O∗) can be continuously removed via the BCFZ membrane once it is generated from NO decomposition, which will result not only in a kinetic acceleration of NO decomposition, but also in the prevention of NO_2 formation. **Table 5** shows the NO conversion for different temperatures.

3.01.5 Conclusions
s0070

There are numerous examples for the application of p0240 membranes to enhance a chemical reaction, such as a dehydrogenation, partial oxidation, isomerization, or an esterification. The traditional concept for an application [AU8] of membranes in reactors is focused on conversion enhancement by equilibrium displacement removing under equilibrium controlled reaction kinetics conditions small product molecules like hydrogen or water, thus increasing the conversion and the yield of a dehydration or dehydrogenation, respectively. The corresponding reactor is called membrane extractor reactor.

By dosing one of the educts selectively or nonselec- p0245 tively through the reactor wall, the partial pressure of this reactant can be fine-tuned along a reactor dimension. Thus, the selectivity of a kinetically controlled

t0025 **Table 5** Conversion of NO at different temperatures without and with oxygen removal using methane as oxygen consuming sweep gas

Temperature (°C)	(a): X(NO) (%) without O$_2$ removal	(b): X(NO) (%) with O$_2$ removal
800	1	29
850	1	60
875	1	100
900	3	100
925	3	100

Experimental details–core side: 30 cm^3 min^{-1} ($F_{NO} = 3$ cm^3 min^{-1}, $F_{Ne} = 1$ cm^3 min^{-1}, $F_{He} = 26$ cm^3 min^{-1}); shell side: (a) no sweep gas applied, and (b) methane as oxygen consuming sweep gas, 50 cm^3 min^{-1} ($F_{CH4} = 8$ cm^3 min^{-1}, $F_{He} = 37$ cm^3 min^{-1}, and $F_{H2O} = 5$ cm^3 min^{-1}); 0.5 g Ni-based catalyst packed on shell side [111].

reaction can be influenced via the partial pressure of a component. As a general rule, low partial pressures of oxygen/hydrogen support a partial, instead of a total, oxidation/hydrogenation. The corresponding reactor is called membrane distributor/contactor reactor. The so-called pore-through-flow membrane reactor is a special type of membrane contactor.

p0250   In Section 4, the successful application of an extractor-type membrane reactor in the case of the reaction rate inhibition was dealt with. As an example, the rate inhibition of the NO_x decomposition by the product molecule oxygen was discussed. The new concept allows one to enhance the reaction rate of catalytic processes, where the recombination and/or desorption of one of the reaction products is the rate-limiting step. Using a semipermeable membrane, which facilitates *in situ* removal of an inhibiting species on a catalyst or catalyst support, helps to effectively reduce the surface concentration of the inhibiting species and, therefore, increases the reaction rate.

p0255   Up to now, there are no chemical membrane reactors in high-temperature operation in the chemical industry; fuel cells and biochemical processes are exceptions. It is believed that the use of oxygen-transporting perovskite-type membranes in combination with a catalyst in partial oxidations, and the selective hydrogenation of unsaturated hydrocarbons in the pore-through-flow membrane reactor as a special case of a catalytic membrane contactor are promising candidates for incipient industrial applications of catalytic membrane reactors.

References

[1] Koros, W. J., Ma, Y. H., Shimidzu, T. *Terminology for Membranes and Membrane Processes*; IUPAC Recommendations from 1996, http://www.che.utexas.edu/nams/IUPAC/iupac.html (accessed December 2009).   b0005

[2] Dittmeyer, R., Caro, J. Catalytic Membrane Reactors. In *Handbook of Heterogeneous Catalysis*, 2nd edn.; Ertl, G., Knözinger, H., Schüth, F., Weitkamp, J., Eds.; Wiley-VCH: Weinheim, 2008; pp 2198–2248.   b0010

[3] Sanchez-Marcano, J. G., Tsotsis, T. T. *Catalytic Membranes and Membrane Reactors*; Wiley-VCH: Weinheim, 2002.   b0015

[4] Paglieri, S. N., Way, J. D. *Sep. Purif. Methods* **2002**, *31*, 1.   b0020

[5] Kemmere, M. F., Keurentjes, J. T. F. Industrial Membrane Reactors. In *Membrane Technology in the Chemical Industry*; Nunes, S. P., Peinemann, K. V., Eds.; Wiley-VCH: Weinheim, 2001; Chapter 5, pp 229–258.   b0025

[6] Liu, S., Tan, X., Li, K., Hughes, R. *Catal. Rev. Sci. Eng.* **2001**, *43*, 147.   b0030

[7] Maschmeyer, T., Jansen, K., Thomas, J. M., Eds. *Top. Catal.* **2004**, *29*.   b0035

[8] Dittmeyer, R., Höllein, V., Daub, K. *J. Mol. Catal. A: Chem.* **2001**, *173*, 135.   b0040

[9] Emig, G., Liauw, M. A. *Top. Catal.* **2002**, *21*, 11.   b0045

[10] Dixon, A. G. *Int. J. Chem. React. Eng.* **2003**, *1*, R6.   b0050

[11] Coronas, J., Santamaria, J. *Top. Catal.* **2004**, *29*, 29.   b0055

[12] Drioli, E., Romano, M. *Ind. Eng. Chem. Res.* **2001**, *40*, 1277.   b0060

[13] Julbe, A., Farusseng, D., Guizard, C. *Catal. Today* **2005**, *104*, 102.   b0065

[14] Julbe, A., Farusseng, D., Guizard, C. *J. Membr. Sci.* **2001**, *181*, 3.   b0070

[15] Drioli, E., Criscuoli A., Curcio, E. *Membrane Contactors: Fundamentals, Applications and Potentialities*; Membrane Science and Technology Series 11; Elsevier: Amsterdam, 2006.   b0075

[16] Seidel-Morgenstern, A. Analysis and Experimental Investigation of Catalytic Membrane Reactors. In *Integrated Chemical Processes*; Sundmacher, K., Kienle, A., Seidel-Morgenstern, A., Eds.; Wiley-VCH: Weinheim, 2005; pp 359–392.   b0080

[17] Caro, J., Caspary, K. J., Hamel, C., *et al. Ind. Eng. Chem. Res.* **2007**, *46*, 2286.   b0085

[18] Drioli, E., Giorno, L. *Biocatalytic Membrane Reactors: Applications in Biotechnology and the Pharmaceutical Industry*; Taylor and Francis: London, 1999.   b0090

[19] Rios, G. M., Belleville, M. P., Paolucci, D., Sanchez, J. *J. Membr. Sci.* **2004**, *242*, 189.   b0095

[20] Coronas, J., Santamaria, J. *Top. Catal.* **2004**, *29*, 29.   b0100

[21] Illgen, U., Schäfer, R., Noack, M., Kölsch, P., Kühnle, A., Caro, J. *Catal. Commun.* **2001**, *2*, 339.   b0105

[22] Schäfer, R., Noack, M., Kölsch, P., Stöhr, M., Caro, J. *Catal. Today* **2003**, *82*, 15.   b0110

[23] Ciavarella, P., Casanave, D., Moueddeb, H., Miachon, S., Fiaty, K., Dalmon, J.-A. *Catal. Today* **2001**, *67*, 177.   b0115

[24] Alshebani, A., Landrivon, E., Schiestel, T., Miachon, S., Dalmon, J.-A. *Proceedings of the 4th International Zeolite Membrane Meeting*, Zaragoza, Spain, July 2007; p 67.   b0120

b0125 [25] Corma, A., Rey, F., Rius, J., Sabater, M., Valencia, S. *Nature* **2004**, *431*, 287.

b0130 [26] Tiscornia, I., Valencia, S., Corma, A., Téllez, C., Coronas, J., Santamaria, J. *Proceedings of the 4th International Zeolite Membrane Meeting*, Zaragoza, Spain, July 2007; p 78.

b0135 [27] Karanikolos, G. N., Stoeger, J., Wydra, J. W., Garcia, H., Corma, A., Tsapatsis, M. *Proceedings of the 4th International Zeolite Membrane Meeting*, Zaragoza, Spain, July 2007; p 61.

b0140 [28] Kiyozumi, Y., Nemoto, Y., Nishide, T., Nagase, T., Hasegawa, Y. *Proceedings of the 4th International Zeolite Membrane Meeting*, Zaragoza, Spain, July 2007; p 57.

b0145 [29] Kita, H., Li, X., Nagamatsu, T., Tanaka, K. *Proceedings of the 4th International Zeolite Membrane Meeting*, Zaragoza, Spain, July 2007; p 18.

b0150 [30] Yajima, K., Nakayama, K., Niino, M., Tomita, T., Yoshida, S. *Proceedings of the 9th International Conference on Inorganic Membranes (ICIM-9),* Lillehammer, Norway, SINTEF, 2006; p 401.

b0155 [31] Espinoza, R. L., Du Toit, E., Santamaria, J. M., Menendez, M. A., Coronas, J., Irusta, S. *Stud. Surf. Sci. Catal.* **2000**, *130*, 389.

b0160 [32] Rohde, M. P., Unruh, D., Schaub, G. *Ind. Eng. Chem. Res.* **2005**, *44*, 9653.

b0165 [33] Rohde, M. P., Schaub, G., Khajavi, S., Jansen, J. C., Kapteijn, F. *Proceedings of the 4th International Zeolite Membrane Meeting*, Zaragoza, Spain, July 2007; p 49.

b0170 [34] Zhu, W., Gora, L., van den Berg, A. W. C., Kapteijn, F., Jansen, J. C., Moulijn, J. A. *J. Membr. Sci.* **2005**, *253*, 57.

b0175 [35] Khajavi, S., Jansen, J. C., Kapteijn, F. *Stud. Surf. Sci. Catal.* **2007**, *170*, 1028.

b0180 [36] Caro, J., Noack, M., Kölsch, P. *Adsorption* **2005**, *11*, 215.

b0185 [37] Kwan, M. S. M., Leung, A. Y. L., Yeung, K. L. *Proceedings of the 4th International Zeolite Membrane Meeting,* Zaragoza, Spain, July 2007; p 15.

b0190 [38] Jensen, K. F. *Chem. Eng. Sci.* **2001**, *56*, 293.

b0195 [39] Wan, Y. S. S., Chau, J. L. H., Yeung, K. L., Gavriilidis, A. *Microporous Mesoporous Mater.* **2001**, *42*, 157.

b0200 [40] Chau, J. L. H., Wan, Y. S. S., Gavriilidis, A., Yeung, K. L. *Chem. Eng. J.* **2002**, *88*, 187.

b0205 [41] Chau, J. L. H., Yeung, K. L. *Chem. Commun.* **2002**, *9*, 960.

b0210 [42] Chau, J. L. H., Leung, A. Y. L., Yeung, K. L. *Lab-on-a-Chip* **2003**, *3*, 53.

b0215 [43] Leung, A. Y. L., Yeung, K. L. *Chem. Eng. Sci.* **2004**, *59*, 4809.

b0220 [44] Leung, A. Y. L., Yeung, K. L. *Stud. Surf. Sci. Catal.* **2004**, *154*, 671.

b0225 [45] Lai, S. M., Martin-Aranda, R., Yeung, K. L. *Chem. Commun.* **2003**, *2*, 218.

b0230 [46] Lai, S. M., Ng C. P., Martin-Aranda, R., Yeung, K. L. *Microporous Mesoporous Mater.* **2003**, *66*, 239.

b0235 [47] Zhang, X. F., Lai, S. M., Martin-Aranda, R., Yeung, K. L. *Appl. Catal. A* **2004**, *261*, 109.

b0240 [48] Yeung, K. L., Zhang, X. F., Lau, W. N., Martin-Aranda, R. *Catal. Today* **2005**, *110*, 26.

b0245 [49] Lau, W. N., Yeung, K. L., Zhang, X. F., Martin-Aranda, R. *Stud. Surf. Sci. Catal.* **2007**, *170*, 1460.

b0250 [50] Wan, Y. S. S., Yeung, K. L., Gavriilidis, A., van Steen, E., Callanan, L. H., Claeys M., *Eds. Stud. Surf. Sci. Catal.* **2004**, *154*, 285.

b0255 [51] Wan, Y. S. S., Yeung, K. L., Gavriilidis, A. *Appl. Catal. A* **2005**, *281*, 285.

b0260 [52] Jiang, H., Wang, H. H., Schiestel, T., Werth, S., Caro, J. *Angew. Chemie* **2008**, *120*, 9481.

b0265 [53] Balachandran, U., Lee, T. H., Wang, S., Dorris, S. E. *Int. J. Hydrogen Energy* **2004**, *29*, 291.

b0270 [54] Balachandran, U., Lee, T. H., Dorris, S. E. *Int. J. Hydrogen Energy* **2007**, *32*, 4451.

b0275 [55] Ramos, R., Menendez, M., Santamaria, J. *Catal. Today* **2000**, *56*, 239.

[56] Alonso, M., Lorences, M. J., Pina, M. P., Patience, G. S. *Catal. Today* **2001**, *67*, 151. b0280

[57] Miachon, S., Dalmon, J.-A. *Top. Catal.* **2004**, *29* 59. b0285

[58] Mota, S., Volta, J.-C., Vorbeck, G., Dalmon, J.-A. *J. Catal.* **2000**, *193*, 319. b0290

[59] Kölsch, P., Smejkal, Q., Noack, M., Schäfer, R., Caro, J. *Catal. Commun.* **2002**, *3*, 465. b0295

[60] Koh, A., Chen, L., Johnson, B., Khimyak, T., Leong, W., Lin, J., *Presented at the 1st World Hydrogen Technologies Convention (WHTC-1)*, Singapore, 3–5 October 2005. b0300

[61] Dyer, P. N., Richards, R. E., Russek, S. L., Taylor, D. M. *Solid State Ion.* **2000**, *134*, 21. b0305

[62] Wang, H. H., Cong, Y., Yang, W. S. *J. Membr. Sci.* **2002**, *210*, 259. b0310

[63] Tan, X. Y., Liu, Y. T., Li, K. *AIChE J.* **2005**, *51*, 1991. b0315

[64] Liu, S. M., Gavalas, G. R. *J. Membr. Sci.* **2005**, *246*, 103. b0320

[65] Van Hassel Prasad, R., Chen, J., Lane, J. Ion-Transport Membrane Assembly Incorporating Internal Support. US Pat. 6,565,632, 2001. b0325

[66] Armstrong, P. A., Bennet, D. L., Foster, E. P. T., van Stein, E. E. Ceramic Membrane Development for Oxygen Supply to Gasification Applications. In *Proceedings of the Gasification Technology Conference*, San Francisco, CA, USA, 27–30 October 2002. b0330

[67] Armstrong, P. A., Sorensen, J., Foster, E. P. T. ITM Oxygen: An Enabler for IGCC. In *Proceedings of the Gasification Technology Conference*, San Francisco, CA, 12–15 October 2003. b0335

[68] Armstrong, P. A., Bennet, D. L., Foster, E. P. T., van Stein, E. E. ITM Oxygen for Gasification. In *Proceedings of the Gasification Technology Conference*, Washington, DC, USA, 3–6 October 2004. b0340

[69] Bruun, T. *Design Issues for High Temperature Ceramic Membrane Reactors. In Proceedings of the 6th International Catalysis in Membrane Reactors,* Lahnstein, Germany, 2004. b0345

[70] Vente, J. F., Haije, W. G., Ijpelaan, R., Rusting, F. T. *J. Membr. Sci.* **2006**, *278*, 66. b0350

[71] Tan, X., Liu, Y., Li, K. *AIChE J.* **2005**, *51*, 1991. b0355

[72] Tan, X., Liu, Y., Li, K. *Ind. Eng. Chem. Res.* **2005**, *44*, 61. b0360

[73] Liu, S., Gavalas, G. R. *J. Membr. Sci.* **2005**, *246*, 103. b0365

[74] Liu, S., Gavalas, G. R. *Ind. Eng. Chem. Res.* **2005**, *44*, 7633. b0370

[75] Tong, J. H., Yang, W. S., Cai, R., Zhu, B. C., Lin, L. W. *Catal. Lett.* **2002**, *78*, 129. b0375

[76] Schiestel, T., Kilgus, M., Peter, S., Caspary, K. J., Wang, H. H., Caro, J. *J. Membr. Sci.* **2005**, *258*, 1. b0380

[77] Tablet, C., Grubert, G., Wang, H. H., *et al. Catal. Today* **2005**, *104*, 126. b0385

[78] Caro, J., Wang, H. H., Tablet, C., *et al. Catal. Today* **2006**, *118*, 128. b0390

[79] Chen, C. S., Feng, S. J., Ran, S., Zhu, D. C., Lin, W., Bouwmeester, H. J. M. *Angew. Chem. Int. Ed.* **2003**, *42*, 5196. b0395

[80] Kondratenko, E. V., Baerns, M. Synthesis Gas Generation by Heterogeneous Catalysts. In *Encyclopedia of Catalysis*; Horvyth, I., Ed.; Wiley: New York, 2003; Vol. 6, pp 424–456. b0400

[81] Wang, H. H., Tablet, C., Schiestel, T., Werth, S., Caro, J. *Catal. Commun.* **2006**, *7*, 907. b0405

[82] Wang, H. H., Caro, J., Werth, S., Schiestel, T. *Angew. Chem. Int. Ed.* **2005**, *44*, 2. b0410

[83] Hamel, C., Seidel-Morgenstern, A., Schiestel, T., *et al. AIChE J.* **2006**, *52*, 3118. b0415

[84] Wang, H. H., Tablet, C., Schiestel, T., Caro, J. *Catal. Today* **2006**, *118*, 98. b0420

[85] Mulla, S. A. R., Buyevskaya, O. V., Baerns, M. *J. Catal.* **2001**, *197*, 43. b0425

b0430 [86] Watson, R. B., Ozkan, U. S. *J. Catal.* **2000**, *191*, 12.

b0435 [87] Mitchell, P. C. H., Wass, S. A. *Appl. Catal. A* **2002**, *225*, 153.

b0440 [88] Brückner, A., Rybarczyk, P., Kosslick, H., Wolf, G.-U., Baerns, M. *Stud. Surf. Sci. Catal.* **2002**, *142*, 1141.

b0445 [89] Wang, H. H., Cong, Y., Yang, W. *Chem. Commun.* **2002**, *14*, 1468.

b0450 [90] Wang, H. H., Cong, Y., Yang, W. *Catal. Lett.* **2002**, *84*, 101.

b0455 [91] Rebeilleau, M., van Veen, A. C., Farrusseng, D., *et al.* *Stud. Surf. Sci. Catal.* **2004**, *147*, 655.

b0460 [92] Rebeilleau, M., Rosini, S., van Veen, A. C., Farrusseng, D., Mirodatos, C. *Catal. Today* **2005**, *104*, 131.

b0465 [93] Akin, F. T., Lin, Y. S. *J. Membr. Sci.* **2002**, *209*, 457.

b0470 [94] Wang, H. H., Cong, Y., Zhu, X., Yang, W. *React. Kinet. Catal. Lett.* **2003**, *79*, 351.

b0475 [95] Akin, F. T., Lin, Y. S. *Catal. Lett.* **2002**, *78*, 239.

b0480 [96] Shao, Z., Dong, H., Xiong, G., Cong, Y., Yang, W. *J. Membr. Sci.* **2001**, *183*, 181.

b0485 [97] Lu, Y., Dixon, A. G., Moser, W. R., Ma, Y., Balachandran, U. *Catal. Today* **2000**, *56*, 297.

b0490 [98] Wang, H. H., Tablet, C., Caro, J. *J. Membr. Sci.* **2008**, *322*, 214.

AU9 b0495 [99] Caro, J., Wang, H. H., Noack, M., *et al.* EP 06 112 764.3,
AU10   18 April 2007.

[100] Caro, J., Wang, H. H., Noack, M., *et al.* Composite   b0500
Membrane. WO 2007/118902 A2, 25 October 2007.

[101] Dittmeyer, R., Svajda, K., Reif, M. *Top. Catal.* **2004**, *29*, 3. b0505

[102] Ilinich, O. M., Cuperus, F. P., Nosova, L. V., Gribov, E. N. b0510
Catal. Today **2000**, *56*, 137.

[103] Ilinich, O. M., Gribov, E. N., Simonov, P. A. *Catal. Today* b0515
2003, *82*, 49.

[104] Reif, M., Dittmeyer, R. *Catal. Today* **2003**, *82*, 3.   b0520

[105] Fritsch, D., Bengtson, G. *Catal. Today* **2006**, *118*, 121. b0525

[106] Schmidt, A., Haidar, R., Schomäcker, R. *Catal. Today* b0530
2005, *104*, 305.

[107] Schomäcker, R., Schmidt, A., Frank, B., Haidar, R., b0535
Seidel-Morgenstern, A. *Chem. Ing. Tech.* **2005**, *77*, 549.

[108] Jiang, H., Wang, H. H., Liang, F., Werth, S., Schiestel, T., b0540
Caro, J. *Angew. Chem. Int. Ed.* **2009**, *48*, 2983.

[109] Bulushev, D. A., Kiwi-Minsker, L., Renken, A. *J. Catal.* b0545
2004, *222*, 389.

[110] Bennici, S., Gervasini, A. *Appl. Catal. B* **2006**, *62*, 336. b0550

[111] Jiang, H., Xing, L., Czuprat, O., *et al.* (in press).   b0555 AU11

[112] Burch, R. *Top. Catal.* **2003**, *24*, 97.   b0560

[113] Burch, R., Millington, P. R., Walker, A. P. *Appl. Catal. B* b0565
1994, *4*, 65.

Biographical Sketch

J. Caro is currently a C4-Professor of physical chemistry at Leibniz University, Hannover, Germany, and the director of the Institute for Physical Chemistry and Electrochemistry. Between 1970 and 1973, he studied chemistry at Leipzig University; he received his PhD in 1977 from the Physics Department of Leipzig University on molecular diffusion of guest molecules in porous media by nuclear magnetic resonance (NMR) methods, supervised by Profs. Kärger and Pfeifer. Later, he worked at the Academy of Sciences in Berlin-Adlershof in adsorption, permeation, and catalysis. In 2001, he was appointed the chair of physical chemistry at Hannover University. During 2005–06, he was the president of the German Catalysis Society. During 2003–06, he was the speaker of the Lighthouse Project of the German Research Ministry 'Membranes for catalysis' (with 12 partners from industry and academia) under the auspices of Das Kompetenznetzwerk Katalyse (ConNeCat, competence network catalysis). J. Caro is the author of 200 papers, 37 patents, and the member of the editorial boards of five journals (e.g., *Advanced Materials*, *Microporous and Mesoporous Materials*, and *Catalysis Communications*).